Role of PHOSPHO1 in periodontal development and function

Role of PHOSPHO1 in periodontal development and function

L. Zweifler[1], M. Ao[2], M. Yadav[3], P. Kuss[3], S. Narisawa[3], T. Kolli[1], H. F. Wimer[4,5], C. Farquharson[6], M.J. Somerman[2], J.L. Millán[3], B.L.Foster[1]

[1] Division of Biosciences, College of Dentistry, The Ohio State University, Columbus, OH, USA
[2] National Institute of Arthritis and Musculoskeletal and Skin Diseases (NIAMS), National Institutes of Health (NIH), Bethesda, MD, USA
[3] Sanford Children's Health Research Center, Sanford Burnham Prebys Medical Discovery Institute, La Jolla, CA, USA
[4] Department of Vertebrate Zoology, National Museum of Natural History, Smithsonian Institution, Washington, DC, USA
[5] National Institute of Dental and Craniofacial Research (NIDCR), National Institutes of Health (NIH), Bethesda, MD, USA
[6] The Roslin Institute and Royal (Dick) School of Veterinary Studies, The University of Edinburgh, Easter Bush, Midlothian EH25 9RG, UK

Corresponding author:
Brian L. Foster
305 W. 12th Avenue
4163 Postle Hall
Division of Biosciences
College of Dentistry
The Ohio State University
Columbus, OH 43210
Phone: 614-247-5760
Email: foster.1004@osu.edu

Words in abstract: 294
Total words: 3,088
References: 33
Figures: 5 figures
Tables: 0 tables
Supplemental Materials: 1 supplemental table and 7 supplemental figures

Running title: PHOSPHO1 and tooth root development

Key words: cementum, dentin, bone, periodontal ligament, extracellular matrix

ABSTRACT

The tooth root and periodontal apparatus, including acellular and cellular cementum, periodontal ligament (PDL), and alveolar bone, are critical for tooth function. Cementum and bone mineralization is regulated by factors including enzymes and extracellular matrix proteins that promote or inhibit hydroxyapatite crystal growth. Orphan Phosphatase 1 (*Phospho1*, PHOSPHO1) is a phosphatase expressed by chondrocytes, osteoblasts, and odontoblasts that functions in skeletal and dentin mineralization by initiating deposition of hydroxyapatite inside membrane-limited matrix vesicles (MVs). The role of PHOSPHO1 in periodontal formation remains unknown and we aimed to determine its functional importance in these tissues. We hypothesized the enzyme would regulate proper mineralization of the periodontal apparatus. Spatiotemporal expression of PHOSPHO1 was mapped during periodontal development, and *Phospho1*$^{-/-}$ mice were analyzed using histology, immunohistochemistry, *in situ* hybridization, radiography, and microcomputed tomography. *Phospho1* gene and PHOSPHO1 protein were expressed by active alveolar bone osteoblasts and cementoblasts during cellular cementum formation. In *Phospho1*$^{-/-}$ mice, acellular cementum formation and mineralization were unaffected while cellular cementum deposition increased, though displayed delayed mineralization and cementoid. *Phospho1*$^{-/-}$ mice featured disturbances in alveolar bone mineralization, shown by accumulation of unmineralized osteiod matrix and interglobular patterns of protein deposition. Parallel to other skeletal sites, deposition of mineral-regulating protein osteopontin (OPN) was increased in alveolar bone in *Phospho1*$^{-/-}$ mice. In contrast to the skeleton, genetic ablation of *Spp1,* the gene encoding OPN*,* did not ameliorate dentoalveolar defects in *Phospho1*$^{-/-}$ mice. Despite alveolar bone mineralization defects, periodontal attachment and function appeared undisturbed in *Phospho1*$^{-/-}$ mice, with normal PDL architecture and no evidence of bone loss over time. This study highlights the role of PHOSPHO1 in mineralization of alveolar bone and cellular cementum, further

revealing that acellular cementum formation is not substantially regulated by PHOSPHO1 and likely does not rely on matrix MV-mediated initiation of mineralization.

INTRODUCTION

The periodontal apparatus, including acellular and cellular cementum, periodontal ligament (PDL), and alveolar bone, are critical for tooth attachment and function (Foster et al. 2007). Mineralization of dentin, cementum, and bone is regulated by several factors, including enzymes that modulate local inorganic phosphate (P_i) and pyrophosphate (PP_i) concentrations, and extracellular matrix (ECM) proteins that promote or inhibit hydroxyapatite crystal growth (Foster et al. 2015a; Foster et al. 2012). While common mineralization regulators are expressed amongst these tissues, local differences in timing and expression levels provide tissue-specific regulatory mechanisms.

Orphan Phosphatase 1 (*Phospho1*, PHOSPHO1), a member of the haloacid dehalogenase superfamily of hydrolases, is expressed by chondrocytes, osteoblasts, and odontoblasts, and has an indispensable role in skeletal mineralization. PHOSPHO1 is proposed to initiate deposition of crystalline hydroxyapatite inside cell-derived membrane limited matrix vesicles (MVs) by generating P_i from hydrolysis of MV membrane constituents, phosphoethanolamine and phosphocholine (Houston et al. 2004; Macrae et al. 2010; McKee et al. 2013; Roberts et al. 2007; Stewart et al. 2006; Stewart et al. 2003). *Phospho1*$^{-/-}$ mice feature scoliosis, osteomalacia, bowed long bones, and spontaneous fractures (Rodriguez-Florez et al. 2015; Yadav et al. 2011). The early role of PHOSPHO1 in mineralization is distinct from that of tissue non-specific alkaline phosphatase (*Alpl;* TNAP), which reduces local concentrations of mineral inhibitor PP_i. While individually knocking out either *Phospho1* or *Alpl* reduces skeletal mineralization, simultaneous ablation of both causes complete absence of mineralization in osteoblast cultures and developing embryos (Huesa et al. 2015; Yadav et al. 2011). *Phospho1*$^{-/-}$ mice also feature increased

expression of ECM protein osteopontin (*Spp1*; OPN), contributing to inhibition of skeletal mineralization (Yadav et al. 2014).

Previously, we demonstrated that PHOSPHO1 is expressed by odontoblasts and functions in mineralization of mouse incisor dentin (McKee et al. 2013). However, the role of PHOSPHO1 in periodontogenesis remains unknown, and we aimed to determine its importance in formation and function of the periodontium. We mapped spatiotemporal expression of PHOSPHO1, analyzed postnatal tooth development in *Phospho1*$^{-/-}$ mice, and evaluated the potential pathological role for increased OPN in the dentition of *Phospho1*$^{-/-}$ mice.

MATERIALS AND METHODS

Mice

Animal procedures were performed in accordance with guidelines of the Animal Care and Use Committee at the Sanford Burnham Prebys Medical Discovery Institute (La Jolla, CA, USA) and National Institutes of Health (Bethesda, MD, USA). To detect *Phospho1* mRNA and protein expression during tooth development, tissues were collected from C57BL/6 mice at 4, 5, 14, 15, and 26 days postnatal (dpn) (n=3-5 per group). *Phospho1*$^{-/-}$ mice (Yadav et al. 2011) and *Spp1*$^{-/-}$ mice (Rittling et al. 1998) have been described previously. Details on breeding and genotyping are found in the Appendix. For analysis of wild-type (WT), *Phospho1*$^{-/-}$, *Spp1*$^{-/-}$, and *Phospho1*$^{-/-}$; *Spp1*$^{-/-}$ mice, mandibles were collected at 14 dpn (n=3), 30 dpn (n=3-12), and 90 dpn (n=2-6).

Radiography and microcomputed tomography

Hemi-mandibles were scanned in a cabinet X-ray (Faxitron X-ray Corp.) at 30 kV for 40 sec. For microcomputed tomography (micro-CT), formalin-fixed mandibles were scanned on a Scanco Medical

micro-CT 50 (Scanco Medical AG, Brüttisellen, Switzerland) with parameters of 9 μm voxel size, 55 KVp, 145 mA, with 0.36 degrees rotation step (180 degrees angular range) and a 400 ms exposure per view. Exported DICOM files were reoriented using ImageJ software (1.48r) to compare coronal and sagittal planes of section. DICOM stacks were rendered as 3D isoimages using Amira software (version 6.0; FEI, Hillsboro, OR). Quantitative micro-CT analysis was performed as described previously (Foster et al. 2015b), and details are provided in the Appendix. Tissue volume (TV), bone volume (BV), bone volume fraction (BV/TV), bone thickness, and tissue mineral density (TMD) were calculated.

Histology

Mandibles fixed in 10% neutral buffered formalin were prepared for histology by decalcifying in 10% v/v glacial acetic acid, 4% v/v neutral buffered formalin, and 0.85% w/v sodium chloride, and embedding in paraffin prior to making 6 μm serial sections. Sections underwent hematoxylin and eosin (H&E) staining (Foster 2012). Histomorphometry was performed on H&E stained sections using a slide scanner (Leica SCN400F) with Digital Imaging Hub software (Leica Microsystems, Wetzlar, Germany). Details on measurements are provided in the Appendix. To evaluate collagen fiber organization, sections were stained by picrosirius red (Polysciences, Inc., Warrington, PA) as described previously (Foster 2012). Non-decalcified 30 dpn hemi-mandibles were embedded in methyl methacrylate for von Kossa and Goldner's trichrome staining, as described previously (Foster et al. 2013).

Immunohistochemistry and *in situ* hybridization

In situ hybridization (ISH) with a digoxigenin-labeled antisense *Phospho1* cRNA probe was performed on paraffin-embedded sections as previously described (Kuss et al. 2009), with indoxyl-nitroblue tetrazolium (BCIP/NBT) substrate to produce a blue reaction. ISH with an antisense *Spp1* probe was

performed on paraffin-embedded sections and visualized with fast red dye (Advanced Cell Diagnostics, Hayward, CA), using hematoxylin as a counterstain.

Immunohistochemistry (IHC) was performed on paraffin-embedded sections using an avidin-biotinylated peroxidase enzyme complex (ABC) based kit (Vector Labs, Burlingame, CA) with a 3-amino-9-ethylcarbazole (AEC) substrate (Vector Labs) to produce a red reaction (Foster 2012). Hematoxylin was used as the counterstain. Primary antibodies included monoclonal rat IgG anti-human TNAP (R&D Systems, Minneapolis, MN)(Zweifler et al. 2015), polyclonal rabbit anti-mouse bone sialoprotein (BSP; Dr. Renny Franceschi, University of Michigan, Ann Arbor, MI)(Foster 2012), polyclonal LF-175 rabbit anti-mouse OPN (Dr. Larry Fisher, NIDCR, Bethesda, MD) (Foster 2012), and human recombinant Fab monoclonal anti-PHOSPHO1 (AbD Serotec, MorphosysAG, Martinsried/Planegg, Germany)(McKee et al. 2013).

Quantitative polymerase chain reaction (QPCR)

RNA was isolated from long bones (femurs), calvaria, molars, and brain tissues of wild-type (WT) mice at 15 dpn for gene expression analysis. For periodontal tissue mRNA analysis, first mandibular molars were extracted at 5, 14, and 26 dpn (excluding gingiva and bone) and RNA was harvested from attached tissues using a purification kit (RNeasy; Qiagen, Valencia, CA). cDNA was synthesized to perform quantitative PCR (Lightcycler 2.0; Roche Applied Science). Primers used to amplify *Phospho1* (NM_153104.3) transcripts in bones and teeth were: F-GGGTGGATAAGACCGCGTA and R-CTTAACCACCACCTTTAGAAACTGT. Primers used for QPCR of PDL tissues were proprietary sequences included in a PCR array (Qiagen).

Statistical analysis

Mean values were compared by one-way ANOVA or independent samples *t*-tests using GraphPad Prism 6.01 (La Jolla, CA).

RESULTS

PHOSPHO1 is expressed during tooth root and periodontal development

Just prior to molar root formation at 5 days postnatal (dpn), *Phospho1*/PHOSPHO1 was expressed at high levels in newly differentiated odontoblasts (Figure 1A, B). During molar root formation, PHOSPHO1 was localized to regions of alveolar bone remodeling (e.g. the crest), and new root odontoblasts maintained expression, albeit at relatively reduced levels (Figure 1C-F). Minimal *Phospho1* mRNA was detected in the follicle near forming acellular cementum, and PHOSPHO1 protein was undetectable. At completion of root formation, odontoblasts no longer expressed PHOSPHO1 (data not shown), however, mRNA and protein were found in regions of cellular cementum formation (Figure 1G, H). QPCR data from mouse tissues indicated that, like long bone and calvarial bone, molars expressed *Phospho1* mRNA (Figure 1I), likely in odontoblasts. QPCR performed on RNA isolated from PDL tissues confirmed ISH and IHC findings, showing significantly increasing *Phospho1* expression during root formation, at 14 and 26 dpn (Figure 1J). Although ameloblasts showed positive PHOSPHO1 protein localization (Figure 1A, B), no mRNA could be detected by *in situ* hybridization in the enamel organ.

Mineralization of cellular but not acellular cementum is dependent on PHOSPHO1

Because PHOSPHO1 functions in bone and dentin mineralization, we suspected it to perform a similar function in cementum. Acellular cementum is the first type of cementum formed and covers the cervical portions of molar roots. Examination of mandibular first molars in *Phospho1*$^{-/-}$ mice and WT controls at 14, 30, and 90 dpn revealed no apparent deficiency in acellular cementum growth (Figure 2A-F). Histomorphometry confirmed no decrease, and in fact, indicated a trend of increased width in in

acellular cementum of *Phospho1*$^{-/-}$ mouse molars compared to WT controls (Figure 2G, H). OPN immunostaining revealed no delay in acellular cementum initiation in *Phospho1*$^{-/-}$ vs. WT molars (Figure 2A, B insets and Figure 2I). Goldner's trichrome staining performed on undecalcified 30 dpn samples revealed a mineralized acellular cementum layer on the surface of *Phospho1*$^{-/-}$ molar roots, similar in appearance to WT cementum (Figure 2C, D insets).

Cellular cementum is deposited on the apical portions of molar teeth. Analysis of mandibular first molars in *Phospho1*$^{-/-}$ mice and WT controls at 30 and 90 dpn revealed increased deposition of cellular cementum (Figure 3A-H). Histomorphometry confirmed a statistically significant increase in cellular cementum area in *Phospho1*$^{-/-}$ compared to WT molars at 30 dpn, and a similar trend at 90 dpn (Figure 3I). By H&E staining, *Phospho1*$^{-/-}$ cellular cementum showed apparent mineralization delays and 20-30 μm cementoid accumulation at the surface (yellow dotted outlines and arrows in Figure 3D and H), and Goldner's trichrome staining of undecalcified sections confirmed this as cementoid (Insets in Figure 3B and D).

While the function of PHOSPHO1 in incisor dentin at early postnatal ages has been previously examined (McKee et al. 2013), its role in molar formation has not been studied. Because both acellular and cellular cementum form on the surface of dentin, in cementum and periodontal analysis, it is important to understand the status of the underlying dentin. Using radiography, micro-CT, histology, and IHC, we confirmed the importance of PHOSPHO1 in both molar and incisor root dentin, based on delayed dentin mineralization and an abnormal and expanded mantle dentin in *Phospho1*$^{-/-}$ compared to WT mice (Supplemental Figures 2-4).

Alveolar bone mineralization and periodontal function in the absence of PHOSPHO1

Alveolar bone of *Phospho1*$^{-/-}$ mice at early postnatal ages was hypomineralized with accumulation of osteoid on the bone surface (McKee et al. 2013). We wondered whether this defect was limited to early ages, or extended into adulthood with potential effects on periodontal function. By H&E staining, alveolar bone of *Phospho1*$^{-/-}$ mice showed apparent mineralization delays and 20-30 μm or more osteoid accumulation at the alveolar bone crest, even at 90 dpn (Figure 4A-D). The mineralization front in *Phospho1*$^{-/-}$ alveolar bone exhibited a globular pattern (Figure 4A and C, insets), suggesting inhibition of mineralization. Von Kossa staining of undecalcified samples at 30 dpn confirmed the mineralization delay and globular patterning in alveolar bone of *Phospho1*$^{-/-}$ compared to WT mice (Figure 4E-H). IHC for BSP, a mineral-binding ECM protein, revealed a similar globular deposition pattern in alveolar bone of *Phospho1*$^{-/-}$ mice (Figure 4I, K). IHC additionally revealed increased OPN localization in alveolar bone of *Phospho1*$^{-/-}$ mice compared to WT (Figure 4J, L), however, ISH did not indicate increased *Spp1* mRNA in dentoalveolar tissue (Figure 4J, L inserts). Quantitative micro-CT analysis revealed a statistically significant 10% reduction in BV/TV, and a non-significant trend of decreased TMD in alveolar bone of *Phospho1*$^{-/-}$ mice compared to WT (Figure 4M, N). Micro-CT data for all dental tissues are summarized in Supplemental Table 1).

Increased levels of OPN contribute to the pathological skeletal hypomineralization in *Phospho1*$^{-/-}$ mice (Yadav et al. 2014), prompting us to determine whether genetic ablation of OPN would ameliorate defects in *Phospho1*$^{-/-}$ alveolar bone. Histology and micro-CT analysis of *Phospho1*$^{-/-}$; *Spp1*$^{-/-}$ mice showed no qualitative or quantitative improvement in alveolar bone mineralization compared to *Phospho1*$^{-/-}$ mice (Supplemental Figure 5 and Supplemental Table 1). Defects in *Phospho1*$^{-/-}$ molar and incisor dentin were similarly not ameliorated by ablation of *Spp1* (Supplemental Figure 6).

Based on alterations in alveolar bone and cellular cementum mineralization in *Phospho1*$^{-/-}$ mice, we asked whether periodontal function was maintained over time. Picrosirius red staining observed under polarized light indicated apparently normal collagen attachment and organization in 30 and 90 dpn *Phospho1*$^{-/-}$ mice (Figure 5A-D). 2D and 3D micro-CT analysis did not identify obvious alveolar bone loss surrounding *Phospho1*$^{-/-}$ mandibular molars (Figure 5E-J shows 90 dpn samples and Supplemental Figure 7 shows 30 dpn samples). Histomorphometry indicated no signs of vertical or horizontal bone loss (CEJ-ABC distance and alveolar bone width) and indicated no significant changes in PDL width (Figure 5K, L).

DISCUSSION

PHOSPHO1 is a phosphatase that functions in skeletal and dental mineralization by initiating deposition of hydroxyapatite within the lumen of MVs (Houston et al. 2004; Macrae et al. 2010; McKee et al. 2013; Roberts et al. 2007; Stewart et al. 2003). Here we show that PHOSPHO1 is expressed by alveolar bone osteoblasts and cementoblasts during cellular cementum formation. In the absence of PHOSPHO1, mineralization defects were found in alveolar bone and cellular cementum, though acellular cementum was unaffected by loss of PHOSPHO1, and periodontal attachment and function appeared undisturbed. In parallel to skeletal sites (Yadav et al. 2014), OPN deposition, though not mRNA expression, was increased in alveolar bone of *Phospho1*$^{-/-}$ mice. In contrast to the skeleton, ablation of *Spp1* did not ameliorate defects in *Phospho1*$^{-/-}$ dentoalveolar tissues. While this study highlights a role for PHOSPHO1 in the mineralization of periodontal tissues, the loss of PHOSPHO1 does not severely impact periodontal function.

PHOSPHO1 functions in alveolar bone mineralization

Previous studies have shown *Phospho1* gene and PHOSPHO1 protein expression in chondrocytes and osteoblasts of the postcranial skeleton and craniofacial region (Houston et al. 2004; Roberts et al. 2007;

Stewart et al. 2006). Inhibition of PHOSPHO1 activity in chick limbs or genetic ablation of *Phospho1* in mice results in impaired mineralization, confirming a critical and non-redundant role in skeletal development (Huesa et al. 2011; Macrae et al. 2010; Yadav et al. 2011). *Phospho1*$^{-/-}$ mice feature reduced body size, short femurs and tibias, osteomalacia, bowed long bones, increased bone fractures, and scoliosis (Yadav et al. 2011). PHOSPHO1 protein is also expressed in odontoblasts at early postnatal ages, and genetic ablation of *Phospho1* in mice causes delayed dentin mineralization (McKee et al. 2013).

Here we report that PHOSPHO1 is detected in osteoblasts coincident with intramembranous ossification associated with new alveolar bone formation and postnatal remodeling, even into adulthood. In parallel to findings in the postcranial skeleton, *Phospho1*$^{-/-}$ mice exhibited delayed alveolar bone mineralization, accumulation of osteoid, abnormal deposition of ECM proteins indicative of mineralization defects, and significantly reduced BV/TV compared to WT. A previous study revealed that PHOSPHO1 regulated the mechanical properties of tibial bone in an age-dependent manner, with partial correction of bone ductile properties at advanced ages (Javaheri et al. 2015). While consistent bulk mineralization defects were apparent in alveolar bone, the alveolar crest appeared most dramatically affected, with persistent osteoid accumulation. This is consistent with the role of PHOSPHO1 in initiation of mineralization and reports that alveolar bone is among the most rapidly remodeling bone (Beertsen et al. 1997). The alveolar crest, in particular, is continually remodeled in response to mechanical loading of teeth, and we have previously identified mineralization defects at this site in other mouse models of hypomineralization (Foster et al. 2015b; Foster et al. 2013; Zweifler et al. 2015). The continuing importance of PHOSPHO1 in alveolar bone mineralization identifies this protein as a potential factor of interest in ongoing periodontal function and regeneration.

OPN is an ECM protein and member of the Small Integrin Binding Ligand N-Linked Glycoprotein (SIBLING) family (Fisher and Fedarko 2003) capable of functioning as a negative regulator of physiological and pathological mineralization (Boskey 2002; Jono et al. 2000; Yuan et al. 2014). In *Phospho1*$^{-/-}$ mice, Increased expression and deposition of OPN in the skeleton, and increased circulating OPN protein, were shown to contribute to the skeletal pathology in *Phospho1*$^{-/-}$ mice (Yadav et al. 2014). In parallel to other skeletal sites, we detected increased deposition of OPN in alveolar bone of *Phospho1*$^{-/-}$ mice, though there was no evidence of locally increased *Spp1* mRNA by *in situ* hybridization, and quantitative PCR analysis was not performed. These data point towards increased circulating OPN protein as the source for increased deposition in dentoalveolar tissues (VandenBos et al. 1999). In contrast to findings that genetic ablation of *Spp1* partially corrected skeletal mineralization defects, we found no qualitative or quantitative evidence that OPN deficiency ameliorated alveolar bone (or dentin) defects in *Phospho1*$^{-/-}$ mice. This suggests that OPN does not play a significant role in the pathological hypomineralization of *Phospho1*$^{-/-}$ dentoalveolar tissues, prompting questions about whether OPN functions differently at different dental/skeletal sites, and whether and how OPN modulates/is modulated by other mineralization regulators that may confer tissue-specific differences. This underlines the need for further studies on the role of OPN in dentoalveolar development.

A role for PHOSPHO1 in cementogenesis

We found no discernible effect of *Phospho1* knockout on acellular cementum development or function, while cellular cementum exhibited delayed mineralization similar to bone. There is a striking correlation between the mineralization defects in *Phospho1*$^{-/-}$ mice and the known distribution of MVs, which have been found in alveolar bone, dentin, and cellular cementum, but have not been identified in acellular cementum formation (Takano et al. 2000). These observations agree with the known functional importance of PHOSPHO1 in MV-initiated hydroxyapatite mineralization. However, the lack of an

acellular cementum phenotype is striking in another sense; acellular cementum was found to be the most sensitive of dentoalveolar tissues to disturbances of mineralization caused by a number of other factors, (Foster et al. 2015a; Foster et al. 2011; Foster et al. 2012; Foster et al. 2013; Zweifler et al. 2015), but here is resistant to loss of PHOSPHO1. Mouse models with defective cementum and/or alveolar bone attachment due to genetic defects (e.g. *Alpl*$^{-/-}$, *Bsp*$^{-/-}$, and *Dmp1*$^{-/-}$ mice) feature detachment and disorganization of the PDL, widespread osteoclastic destruction of alveolar bone, and a breakdown of periodontal function akin to periodontal disease in humans, in the range of 1-2 months of age (Foster et al. 2015a; Foster et al. 2013; Gasque et al. 2015; Soenjaya et al. 2015; Ye et al. 2008; Zweifler et al. 2015). Though *Phospho1*$^{-/-}$ mice exhibit defective alveolar bone mineralization, no significant periodontal destruction is evident, further confirming that acellular cementum is functional, as is the periodontal complex.

Cellular cementum responded similarly to bone in *Phospho1*$^{-/-}$ mice, exhibiting hypomineralization, cementoid accumulation, and altered morphology, in this case, significant increased deposition. While the proximal cause for increased cellular cementum deposition in *Phospho1*$^{-/-}$ mice remains elusive, two possible mechanisms present themselves. First, alterations in underlying dentin may induce changes in cellular cementum. As we observed previously (McKee et al. 2013), and confirmed and extended in this study, effects of PHOSPHO1 deficiency manifest primarily in the outermost mantle dentin layer that serves as the substrate for cellular cementum deposition. A second mechanism for increased cellular cementum may be compensation resulting from disturbed synthesis and/or compromised mechanical properties. In support of this theory, a very similar increase in hypomineralized cellular cementum has been found when mineralization is disturbed in *Alpl*$^{-/-}$ mice (Zweifler et al. 2015) and mice treated with 1-hydroxyethylidene-1,1-bisphosphonate (Takano et al. 2003). Divergent effects of loss of PHOSPHO1

on acellular vs. cellular cementum further underscore developmental and regulatory differences between these tissues.

ACKNOWLEDGMENTS

The authors declare no conflict of interest. This research was supported by a grant from the National Institute for Dental and Craniofacial Research (NIDCR) of the NIH (DE12889 to JLM), a grant from the BBSRC (BB/J004316/1 to CF), grants from the National Institute of Arthritis and Musculoskeletal and Skin Diseases (NIAMS) of the NIH (AR53102 to JLM and AR066110 to BLF), by the Intramural Research Program of NIAMS (MJS), and by the Dr. Rudy Melfi Fellowship from The Ohio State University (OSU) College of Dentistry (LEZ). The authors thank Nasrin Kalantari Pour (NIAMS/NIH) for histology, Anne Tran and Alyssa Coulter (NIAMS/NIH) for assistance with immunostaining, Kristina Zaal of the NIAMS Light Imaging Section for assistance with slide scanning, Kenn Holmbeck (NIDCR/NIH) for assistance with micro-CT scanning, and Lyudmila Lukashova (Hospital for Special Surgery, Ney York, NY) for assistance with micro-CT analysis.

REFERENCES

Beertsen W, McCulloch CA, Sodek J. 1997. The periodontal ligament: A unique, multifunctional connective tissue. Periodontol 2000. 13:20-40.

Boskey AL. 2002. Variations in bone mineral properties with age and disease. J Musculoskelet Neuronal Interact. 2(6):532-534.

Fisher LW, Fedarko NS. 2003. Six genes expressed in bones and teeth encode the current members of the sibling family of proteins. Connect Tissue Res. 44 Suppl 1:33-40.

Foster BL. 2012. Methods for studying tooth root cementum by light microscopy. Int J Oral Sci. 4(3):119-128.

Foster BL, Ao M, Willoughby C, Soenjaya Y, Holm E, Lukashova L, Tran AB, Wimer HF, Zerfas PM, Nociti FH, Jr. et al. 2015a. Mineralization defects in cementum and craniofacial bone from loss of bone sialoprotein. Bone. 78:150-164.

Foster BL, Nagatomo KJ, Bamashmous SO, Tompkins KA, Fong H, Dunn D, Chu EY, Guenther C, Kingsley DM, Rutherford RB et al. 2011. The progressive ankylosis protein regulates cementum apposition and extracellular matrix composition. Cells Tissues Organs. 194(5):382-405.

Foster BL, Nagatomo KJ, Nociti FH, Fong H, Dunn D, Tran AB, Wang W, Narisawa S, Millán JL, Somerman MJ. 2012. Central role of pyrophosphate in acellular cementum formation. PLoS One. 7(6):e38393.

Foster BL, Popowics TE, Fong HK, Somerman MJ. 2007. Advances in defining regulators of cementum development and periodontal regeneration. Curr Top Dev Biol. 78:47-126.

Foster BL, Sheen CR, Hatch NE, Liu J, Cory E, Narisawa S, Kiffer-Moreira T, Sah RL, Whyte MP, Somerman MJ et al. 2015b. Periodontal defects in the a116t knock-in murine model of odontohypophosphatasia. J Dent Res. 94(5):706-714.

Foster BL, Soenjaya Y, Nociti FH, Holm E, Zerfas PM, Wimer HF, Holdsworth DW, Aubin JE, Hunter GK, Goldberg HA et al. 2013. Deficiency in acellular cementum and periodontal attachment in bsp null mice. J Dent Res. 92(2):166-172.

Gasque KC, Foster BL, Kuss P, Yadav MC, Liu J, Kiffer-Moreira T, van Elsas A, Hatch N, Somerman MJ, Millan JL. 2015. Improvement of the skeletal and dental hypophosphatasia phenotype in alpl(-/-) mice by administration of soluble (non-targeted) chimeric alkaline phosphatase. Bone. 72:137-147.

Houston B, Stewart AJ, Farquharson C. 2004. Phospho1-a novel phosphatase specifically expressed at sites of mineralisation in bone and cartilage. Bone. 34(4):629-637.

Huesa C, Houston D, Kiffer-Moreira T, Yadav MM, Millan JL, Farquharson C. 2015. The functional co-operativity of tissue-nonspecific alkaline phosphatase (tnap) and phospho1 during initiation of skeletal mineralization. Biochemistry and biophysics reports. 4:196-201.

Huesa C, Yadav MC, Finnilä MA, Goodyear SR, Robins SP, Tanner KE, Aspden RM, Millán JL, Farquharson C. 2011. Phospho1 is essential for mechanically competent mineralization and the avoidance of spontaneous fractures. Bone. 48(5):1066-1074.

Javaheri B, Carriero A, Staines KA, Chang YM, Houston DA, Oldknow KJ, Millan JL, Kazeruni BN, Salmon P, Shefelbine S et al. 2015. Phospho1 deficiency transiently modifies bone architecture yet produces consistent modification in osteocyte differentiation and vascular porosity with ageing. Bone. 81:277-291.

Jono S, McKee MD, Murry CE, Shioi A, Nishizawa Y, Mori K, Morii H, Giachelli CM. 2000. Phosphate regulation of vascular smooth muscle cell calcification. Circ Res. 87(7):E10-17.

Kuss P, Villavicencio-Lorini P, Witte F, Klose J, Albrecht AN, Seemann P, Hecht J, Mundlos S. 2009. Mutant hoxd13 induces extra digits in a mouse model of synpolydactyly directly and by decreasing retinoic acid synthesis. J Clin Invest. 119(1):146-156.

Macrae VE, Davey MG, McTeir L, Narisawa S, Yadav MC, Millan JL, Farquharson C. 2010. Inhibition of phospho1 activity results in impaired skeletal mineralization during limb development of the chick. Bone. 46(4):1146-1155.

McKee MD, Yadav MC, Foster BL, Somerman MJ, Farquharson C, Millan JL. 2013. Compounded phospho1/alpl deficiencies reduce dentin mineralization. J Dent Res. 92(8):721-727.

Rittling SR, Matsumoto HN, McKee MD, Nanci A, An XR, Novick KE, Kowalski AJ, Noda M, Denhardt DT. 1998. Mice lacking osteopontin show normal development and bone structure but display altered osteoclast formation in vitro. J Bone Miner Res. 13(7):1101-1111.

Roberts S, Narisawa S, Harmey D, Millan JL, Farquharson C. 2007. Functional involvement of phospho1 in matrix vesicle-mediated skeletal mineralization. Journal of bone and mineral research : the official journal of the American Society for Bone and Mineral Research. 22(4):617-627.

Rodriguez-Florez N, Garcia-Tunon E, Mukadam Q, Saiz E, Oldknow KJ, Farquharson C, Millan JL, Boyde A, Shefelbine SJ. 2015. An investigation of the mineral in ductile and brittle cortical mouse bone. J Bone Miner Res. 30(5):786-795.

Soenjaya Y, Foster BL, Nociti FH, Jr., Ao M, Holdsworth DW, Hunter GK, Somerman MJ, Goldberg HA. 2015. Mechanical forces exacerbate periodontal defects in bsp-null mice. J Dent Res. 94(9):1276-1285.

Stewart AJ, Roberts SJ, Seawright E, Davey MG, Fleming RH, Farquharson C. 2006. The presence of phospho1 in matrix vesicles and its developmental expression prior to skeletal mineralization. Bone. 39(5):1000-1007.

Stewart AJ, Schmid R, Blindauer CA, Paisey SJ, Farquharson C. 2003. Comparative modelling of human phospho1 reveals a new group of phosphatases within the haloacid dehalogenase superfamily. Protein engineering. 16(12):889-895.

Takano Y, Sakai H, Baba O, Terashima T. 2000. Differential involvement of matrix vesicles during the initial and appositional mineralization processes in bone, dentin, and cementum. Bone. 26(4):333-339.

Takano Y, Sakai H, Watanabe E, Ideguchi-Ohma N, Jayawardena CK, Arai K, Asawa Y, Nakano Y, Shuda Y, Sakamoto Y et al. 2003. Possible role of dentin matrix in region-specific deposition of cellular and acellular extrinsic fibre cementum. J Electron Microsc (Tokyo). 52(6):573-580.

VandenBos T, Bronckers A, Goldberg H, Beertsen W. 1999. Blood circulation as source for osteopontin in acellular extrinsic fiber cementum and other mineralizing tissues. J Dent Res. 78(11):1688-1695.

Yadav MC, Huesa C, Narisawa S, Hoylaerts MF, Moreau A, Farquharson C, Millan JL. 2014. Ablation of osteopontin improves the skeletal phenotype of phospho1 mice. J Bone Miner Res.

Yadav MC, Simao AM, Narisawa S, Huesa C, McKee MD, Farquharson C, Millan JL. 2011. Loss of skeletal mineralization by the simultaneous ablation of phospho1 and alkaline phosphatase function: A unified model of the mechanisms of initiation of skeletal calcification. Journal of bone and mineral research : the official journal of the American Society for Bone and Mineral Research. 26(2):286-297.

Ye L, Zhang S, Ke H, Bonewald L, Feng J. 2008. Periodontal breakdown in the dmp1 null mouse model of hypophosphatemic rickets. J Dent Res. 87(7):624-629.

Yuan J, Ju E, Yang J, Chen X, Li H. 2014. Different patterns of puberty effect in neural oscillation to negative stimuli: Sex differences. Cogn Neurodyn. 8(6):517-524.

Zweifler LE, Patel MK, Nociti FH, Wimer HF, Millán JL, Somerman MJ, Foster BL. 2015. Counter-regulatory phosphatases tnap and npp1 temporally regulate tooth root cementogenesis. Int J Oral Sci. 7(1):27-41.

FIGURE CAPTIONS

Figure 1. PHOSPHO1 is expressed in periodontal tissues during development. During tooth root and periodontal development, *Phospho1* mRNA was localized by *in situ* hybridization (ISH; top row) and PHOSPHO1 protein was localized by immunohistochemistry (IHC; second row). **(A, B)** Just prior to initiation of root formation at 4 days postnatal (dpn), ISH and IHC staining of *Phospho1*/PHOSPHO1 shows elevated expression in osteoblasts (Ob) of actively forming alveolar bone (AB), and in newly differentiated odontoblasts (Od) in the first molar tooth. Ameloblasts (Am) show positive IHC staining, but no ISH signal. **(C, D)** During root formation at 14 dpn, highest PHOSPHO1 is localized to regions of AB modeling, with weaker expression in new odontoblasts forming root dentin (DE). Weak mRNA and no protein is detected in apical regions near new acellular cementum (AC), while **(E, F)** neither mRNA nor protein is found near AC on the cervical region of the root. **(G, H)** Cementoblasts (Cb) associated with cellular cementum (CC) formation showed positive staining for both *Phospho1* mRNA and PHOSPHO1 protein. **(M)** *Phospho1* mRNA is detected in mouse long bone (LB), calvarial bone (CB), and molars (MOL) at 15 dpn, though expression in brain (BR) is negligible (n=3 for each). **(N)** QPCR performed on RNA isolated from mouse PDL tissues (n=3) confirms that *Phospho1* expression is detected during root formation at 5, 14, and 26 dpn, with increased expression over time (* $p < 0.05$; ** $p < 0.01$, compared to expression at 5 dpn).

Figure 2. Acellular cementum is not defective in *Phospho1*$^{-/-}$ mice. (A-F) Observation and histomorphometry of H&E stained histological sections of the first mandibular molar at 14, 30, and 90 dpn reveals no defect in acellular cementum (AC) in *Phospho1*$^{-/-}$ compared to WT mice. **(G, H)** Histomorphometry of AC width indicates no deficit in in *Phospho1*$^{-/-}$ mice compared to controls, and a trend for increased AC thickness (* $p < 0.05$; *** $p < 0.001$). Osteopontin (OPN) immunostaining (insets in A, B) indicates no delay in AC initiation in *Phospho1*$^{-/-}$ vs. WT molars at 14 dpn, confirmed by

histomorphometric measurement in **(I)**. Goldner's trichrome staining (insets in C, D) performed on 30 dpn undecalcified samples suggests a similarly mineralized AC layer on *Phospho1*$^{-/-}$ and WT molar roots. Dentin (DE) defects are described in Supplemental Figures 2-4. PDL=Periodontal ligament; AB=Alveolar bone.

Figure 3. Cellular cementum mineralization is delayed in *Phospho1*$^{-/-}$ mice. (A, C, E, G, I) Observation and histomorphometry of H&E stained histological sections of the first mandibular molar at 30 and 90 dpn reveals a trend of increased cellular cementum (CC) deposition in *Phospho1*$^{-/-}$ compared to WT mice (** $p < 0.01$ at 30 dpn). CC perimeter is indicated by red dotted outlines in A, C, E, and G. **(B, D, F, H)** *Phospho1*$^{-/-}$ cellular cementum shows apparent mineralization delays and 20-30 μm cementoid accumulation at the surface (dotted yellow outlines and yellow arrows in D and H), and Goldner's trichrome staining of undecalcified mandible sections at 30 dpn confirms this unmineralized cementoid accumulation (insets in B, D). DE=Dentin; PDL=Periodontal ligament; AB=Alveolar bone.

Figure 4. Persistent alveolar bone defects in *Phospho1*$^{-/-}$ mice. (A-D) Observation of H&E stained histological sections of first mandibular molar regions at 30 and 90 dpn reveals apparent mineralization delays and 20-30 μm of osteoid accumulation at the alveolar bone (AB) crest (indicated by yellow dotted outlines) of *Phospho1*$^{-/-}$ mice compared to controls. The mineralization front in *Phospho1*$^{-/-}$ mouse AB appears globular, indicative of inhibition of mineralization (insets in A, C, yellow arrow in C). **(E-H)** Von Kossa staining of undecalcified samples at 30 dpn confirmed globular mineralization defects (yellow arrows) in *Phospho1*$^{-/-}$ AB compared to WT. **(I, K)** Immunostaining for bone sialoprotein (BSP) reveals a globular deposition pattern in AB of *Phospho1*$^{-/-}$ mice compared to WT. **(J, L)** Immunostaining for osteopontin (OPN) reveals increased localization in AB of *Phospho1*$^{-/-}$ mice compared to WT. Inserts in J and L show that *in situ* hybridization does not indicate increased *Spp1* mRNA expression in alveolar bone

of *Phospho1*$^{-/-}$ mice. Quantitative microCT analysis reveals **(M)** a statistically significant 10% reduction in BV/TV, and **(N)** a non-significant trend of decreased TMD in AB of *Phospho1*$^{-/-}$ mice compared to WT. Micro-CT data for all dental tissues are summarized in Supplemental Table 1. DE=Dentin; PDL=Periodontal ligament.

Figure 5. Loss of PHOSPHO1 does not inhibit periodontal function. (A-D) Observation of picrosirius red stained 30 and 90 dpn tissues under polarized light indicated similar collagen attachment to teeth and alveolar bone (AB), and periodontal ligament (PDL) organization in *Phospho1*$^{-/-}$ and WT control mice. **(E-J)** Analysis of microCT 2D cross sections and 3D renderings at 90 dpn does not indicate AB loss surrounding the mandibular molars (M1, M2, and M3). Insets in I and J show similar alveolar crest height (red dotted line) in *Phospho1*$^{-/-}$ and WT mice. MicroCT results from 30 dpn samples are shown in Supplemental Figure 7. **(K, L)** Histomorphometry confirms similar CEJ-ABC distance, AB width, and PDL width, on buccal and lingual aspects of mandibular M1 in *Phospho1*$^{-/-}$ mice compared to controls ($p > 0.05$ in independent samples t-test). DE=Dentin.

SUPPLEMENTAL DATA

Supplemental Figure 1. Genotyping *Phospho1* and *Spp1* mice. PCR and gel electrophoresis were used for mouse genotyping. Primer sequences are provided in the Appendix Materials and Methods. **(A)** The 355 bp amplicon from *Phospho1* exon 2 was incubated with BsrDI restriction enzyme to identify the intact 355 bp WT band or digested 144 bp and 211 bp fragments due to a point mutation in *Phospho1*$^{-/-}$ mice. **(B)** *Spp1* mice are identified by an 821 bp product for *Spp1*$^{+}$ WT allele, an 1,800 bp product for *Spp1*$^{-}$ null allele, or presence of both products in *Spp1*$^{+/-}$ heterozygote (Het) mice. MW=Molecular weight marker, and numbers to the left of the gel images represent MW band sizes.

Supplemental Figure 2. Developmental dentin defects in *Phospho1*$^{-/-}$ mice at 14 dpn. (A, B) Radiography of the mandible indicates delayed dentin (DE) mineralization of the *Phospho1*$^{-/-}$ mouse incisor (INC), where WT incisor lingual (root) aspect initiates near the second molar (M2; white arrow in panel A) and the *Phospho1*$^{-/-}$ incisor lingual aspect initiates beneath the first molar (M1; yellow arrow in panel B). **(C-J)** Micro-CT analysis indicates delayed DE mineralization (yellow asterisks) and thin incisor dentin (yellow arrow) in *Phospho1*$^{-/-}$ mouse incisors. **(K-N)** By histology, an apparent delay in DE mineralization is observed in the first mandibular molar in H&E stained sections (red boxes in K and M indicate higher magnification panels L and N, respectively). Yellow brackets in panel N vs. L indicate the lag between DE matrix production and mineralization, with a larger distance suggesting delayed DE mineralization in *Phospho1*$^{-/-}$ mice, compared to controls. **(O)** Histomorphometry conducted on H&E stained section confirms significantly delayed DE mineralization (* indicates $p < 0.05$) on the buccal aspect of the first mandibular molar. Other measurements on root DE did not indicate significant differences between *Phospho1*$^{-/-}$ and control mice ($p > 0.05$) at this age. M3=third molar; SAG=sagittal plane; INC=incisor; PDL=periodontal ligament.

Supplemental Figure 3. Developmental dentin defects in *Phospho1*$^{-/-}$ mice at 30 dpn. Radiography, microCT, and histology analysis of *Phospho1*$^{-/-}$ mouse incisors and molars at 30 dpn identify similar dentin defects as are observed at 14 dpn (Supplemental Figure 2). **(A, B)** Radiography of the mandible indicates delayed dentin (DE) mineralization of the *Phospho1*$^{-/-}$ mouse incisor (INC), where WT incisor lingual (root) aspect initiates well behind third molar (M3; white arrow in panel A) and the *Phospho1*$^{-/-}$ incisor lingual aspect initiates beneath the second molar (M2; yellow arrow in panel B). **(C-J)** Micro-CT analysis indicates delayed DE mineralization (yellow asterisks) and thin incisor DE (yellow arrows) in *Phospho1*$^{-/-}$ mouse incisors. **(K-N)** Histology reveals an altered mantle dentin (MD) layer of *Phospho1*$^{-/-}$ vs. WT control mice, including increased width and globular appearance. **(O)** Histomorphometry conducted on H&E stained sections confirms a significantly increased MD layer ($p < 0.05$) in *Phospho1*$^{-/-}$ vs. WT mice, while other DE parameters do not appear different at 30 dpn. M1=first molar; SAG=sagittal plane; PDL=periodontal ligament, AC=acellular cementum.

Supplemental Figure 4. Developmental dentin defects in *Phospho1*$^{-/-}$ mice at 90 dpn. Radiography, microCT, and histology analysis of *Phospho1*$^{-/-}$ mouse incisors and molars at 90 dpn identify similar dentin defects as are observed at 14 and 30 dpn (Supplemental Figures 2 and 3). **(A, B)** Radiography of the mandible indicates delayed dentin (DE) mineralization of the *Phospho1*$^{-/-}$ mouse incisor (INC), where WT incisor lingual (root) aspect initiates well behind third molar (M3; white arrow in panel A) and the *Phospho1*$^{-/-}$ incisor lingual aspect initiates beneath the mesial third molar (M3; yellow arrow in panel B). **(C-J)** Micro-CT analysis indicates delayed DE mineralization (yellow asterisk in panel J) and thin incisor DE (yellow arrows) in *Phospho1*$^{-/-}$ mouse incisors. **(K-N)** Histology reveals an altered mantle dentin (MD) layer of *Phospho1*$^{-/-}$ vs. WT control mice, including increased width and globular appearance. M1=first molar; M2=second molar; SAG=sagittal plane; PDL=periodontal ligament; AB=alveolar bone.

Supplemental Figure 5. Ablation of OPN does not reverse alveolar bone defects from loss of PHOSPHO1. (A, B) Observation of H&E stained histological sections of first mandibular molar regions of *Phospho1*$^{-/-}$; *Spp1*$^{-/-}$ double deficient mice at 30 and 90 dpn reveals mineralization delays and osteoid accumulation at the alveolar bone (AB) crest (indicated by yellow dotted outlines), similar to *Phospho1*$^{-/-}$ mice (see Figure 4). **(C)** Osteopontin (OPN) immunostaining in *Phospho1*$^{-/-}$; *Spp1*$^{-/-}$ double deficient mice identifies a globular deposition pattern similar to *Phospho1*$^{-/-}$ mice (see Figure 4). **(D)** Lack of OPN immunostaining in AB confirms its loss in *Phospho1*$^{-/-}$; *Spp1*$^{-/-}$ double deficient mice. Quantitative microCT analysis of AB reveals **(M)** a statistically significant reduction in BV/TV, and **(N)** a non-significant trend of decreased TMD in in *Phospho1*$^{-/-}$; *Spp1*$^{-/-}$ double deficient mice compared to WT, with no significant difference or apparent improvement compared to *Phospho1*$^{-/-}$ mice. Micro-CT data for all dental tissues are summarized in Supplemental Table 1. DE=Dentin; PDL=Periodontal ligament.

Supplemental Figure 6. Ablation of OPN does not reverse dentin defects from loss of PHOSPHO1. Dentin defects in *Phospho1*$^{-/-}$*;Spp1*$^{-/-}$ double deficient mice are similar to those in *Phospho1*$^{-/-}$ mice (see Supplemental Figures 2-4 for comparison). **(A)** Radiography of the mandible at 14, 30, and 90 dpn, indicates consistently delayed dentin (DE) mineralization of the *Phospho1*$^{-/-}$*;Spp1*$^{-/-}$mouse incisor (INC), where the incisor lingual (root) aspect initiates beneath the first or second molar (M1 or M2, respectively; yellow arrow). **(B)** Micro-CT analysis at 14, 30, and 90 dpn indicates delayed DE mineralization (yellow asterisk at 14 dpn) and thin incisor DE (yellow arrows at 14, 30, and 90 dpn) in *Phospho1*$^{-/-}$*;Spp1*$^{-/-}$mouse INC. **(C)** Histomorphometry conducted on 14 dpn H&E stained sections confirms a significantly larger ($p < 0.05$) lag in *Phospho1*$^{-/-}$*;Spp1*$^{-/-}$molar dentin mineralization (similar to *Phospho1*$^{-/-}$ mice) compared to WT, and a trend for increased mantle dentin thickness in both *Phospho1*$^{-/-}$*;Spp1*$^{-/-}$ and *Phospho1*$^{-/-}$ mice. **(D)** Histomorphometry conducted on 30 dpn H&E stained sections

confirms a trend for increased mantle dentin thickness in both *Phospho1*$^{-/-}$*;Spp1*$^{-/-}$ and *Phospho1*$^{-/-}$ mice. M3=third molar; SAG=sagittal plane.

Supplemental Figure 7. Loss of PHOSPHO1 does not alter periodontal parameters at 30 dpn. (A-F) Analysis of microCT 2D cross sections and 3D renderings at 30 dpn does not identify any measurable alveolar bone (AB) loss surrounding the mandibular molars (M1, M2, and M3). Insets in E and F show similar alveolar crest height (red dotted line) in *Phospho1*$^{-/-}$ and WT mice.

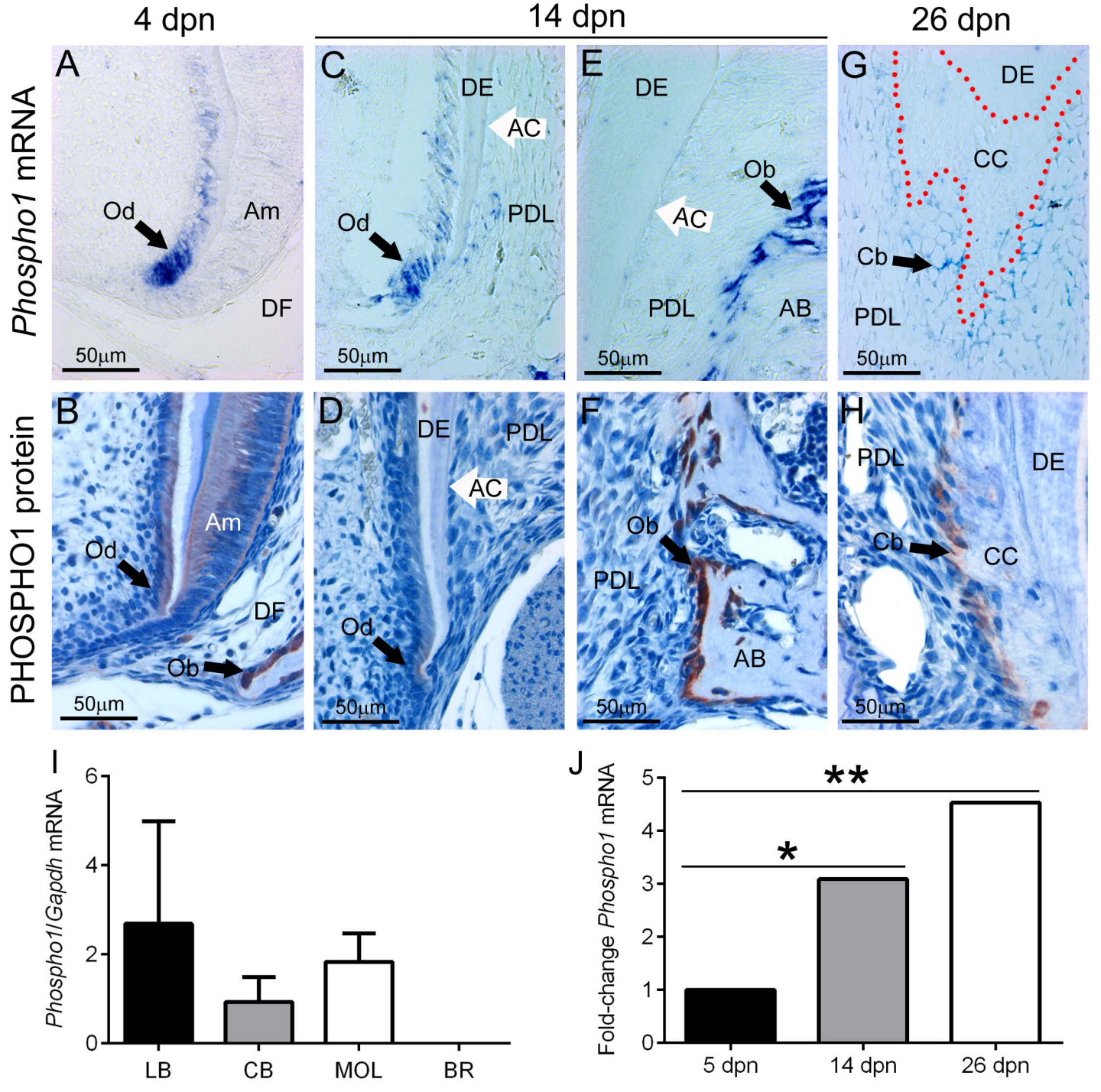
4 dpn
14 dpn
26 dpn
Phospho1 mRNA
PHOSPHO1 protein
A
B
C
D
E
F
G
H
Od
Am
DF
DE
AC
PDL
Ob
AB
Cb
CC
50μm

I
Phospho1/Gapdh mRNA
0
2
4
6
LB
CB
MOL
BR

J
Fold-change Phospho1 mRNA
0
1
2
3
4
5
**
*
5 dpn
14 dpn
26 dpn

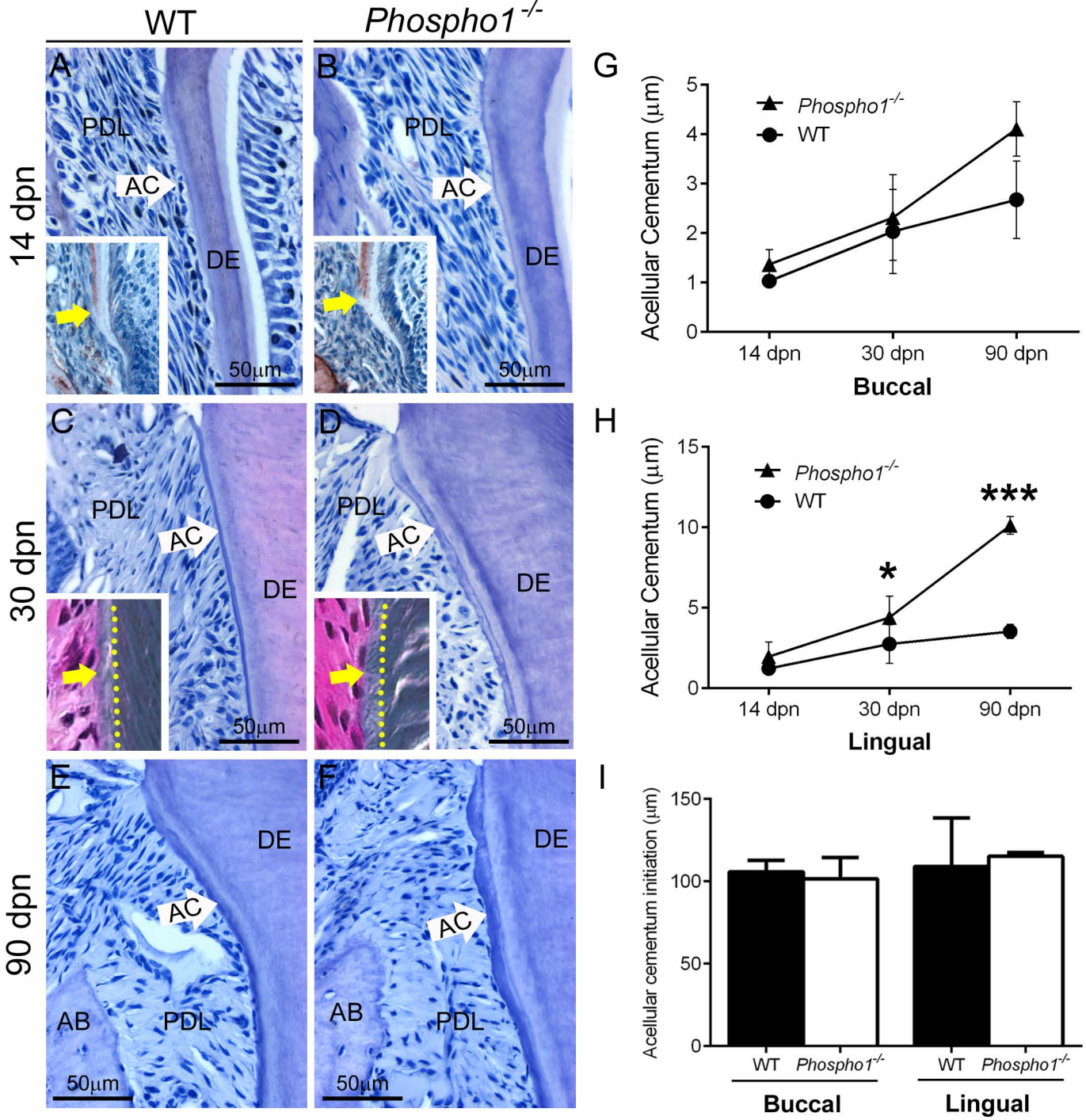
WT
Phospho1 -/-
14 dpn
30 dpn
90 dpn
A
B
C
D
E
F
PDL
AC
DE
AB
50μm
G
H
I
Acellular Cementum (μm)
Phospho1-/-
WT
14 dpn
30 dpn
90 dpn
Buccal
Lingual
*
***
Acellular cementum initiation (μm)
WT
Phospho1-/-
Buccal
Lingual

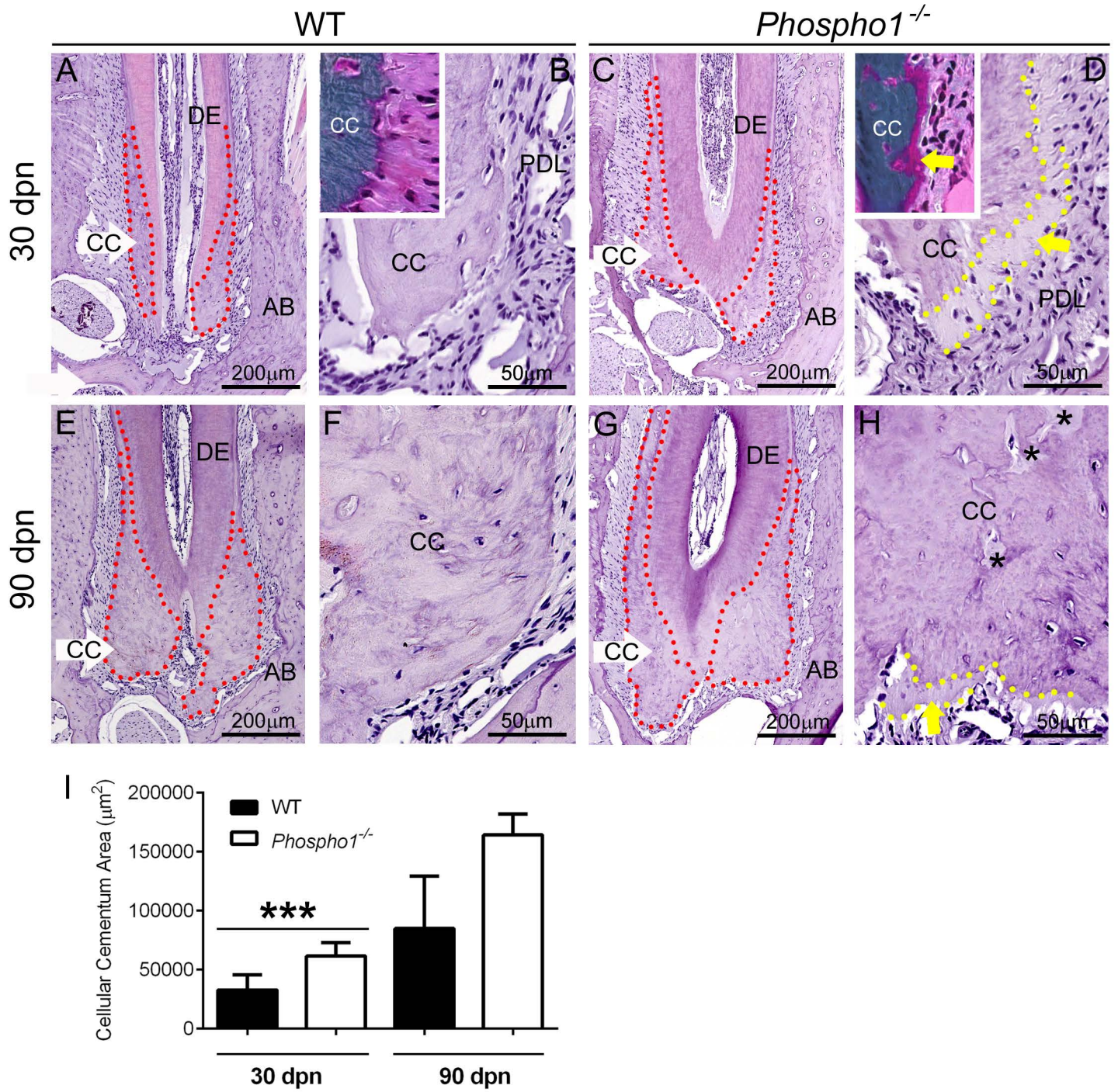
WT
Phospho1 -/-
30 dpn
90 dpn
A
B
C
D
E
F
G
H
DE
CC
AB
PDL
200µm
50µm
*

I
Cellular Cementum Area (µm2)
200000
150000
100000
50000
0
WT
Phospho1 -/-
***
30 dpn
90 dpn

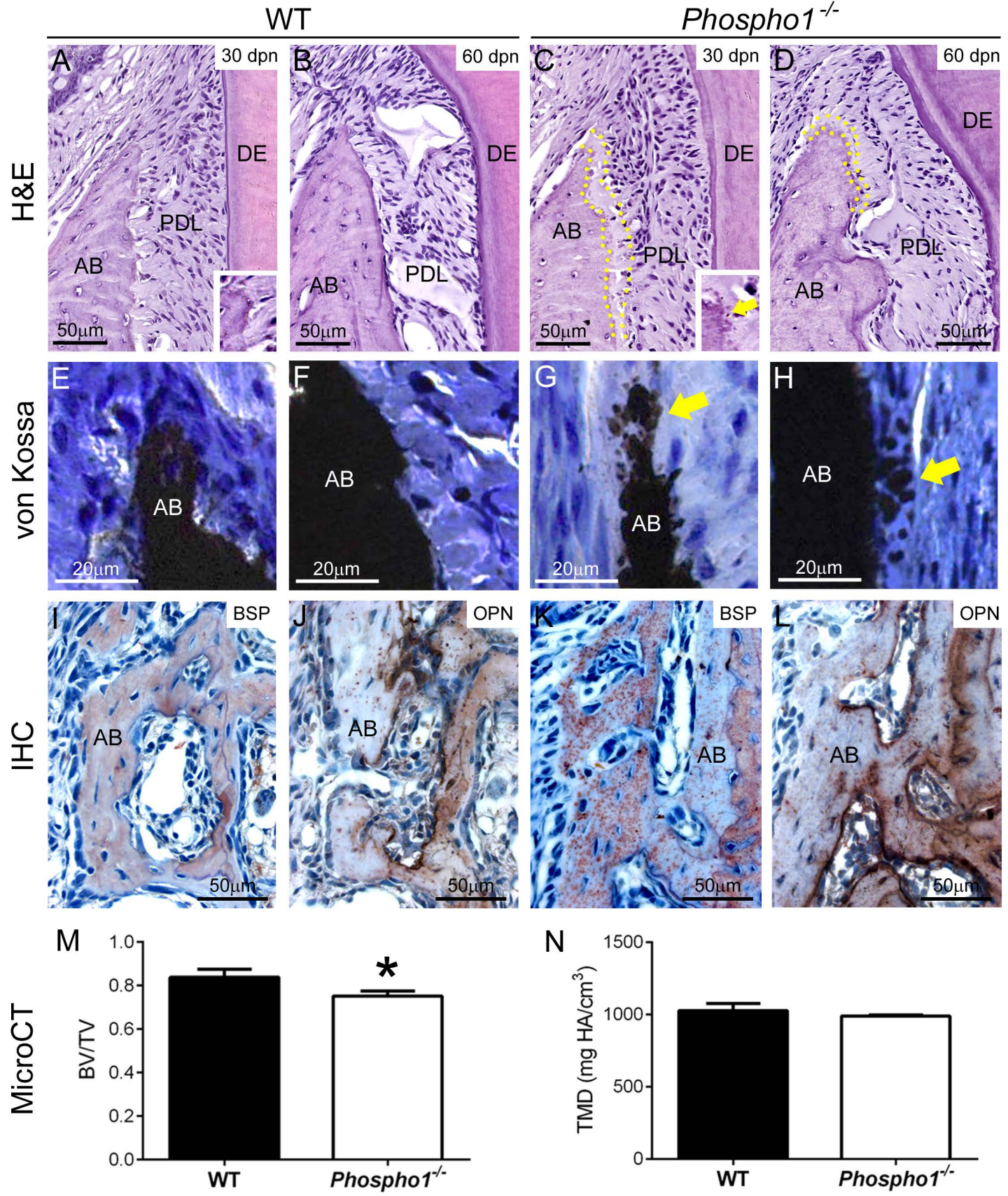
WT
Phospho1 -/-
H&E
A
30 dpn
DE
PDL
AB
50μm
B
60 dpn
DE
AB
PDL
50μm
C
30 dpn
DE
AB
PDL
50μm
D
60 dpn
DE
PDL
AB
50μm
von Kossa
E
AB
20μm
F
AB
20μm
G
AB
20μm
H
AB
20μm
IHC
I
BSP
AB
50μm
J
OPN
AB
50μm
K
BSP
AB
50μm
L
OPN
AB
50μm
MicroCT
M
BV/TV
1.0
0.8
0.6
0.4
0.2
0.0
*
WT
Phospho1 -/-
N
TMD (mg HA/cm3)
1500
1000
500
0
WT
Phospho1 -/-

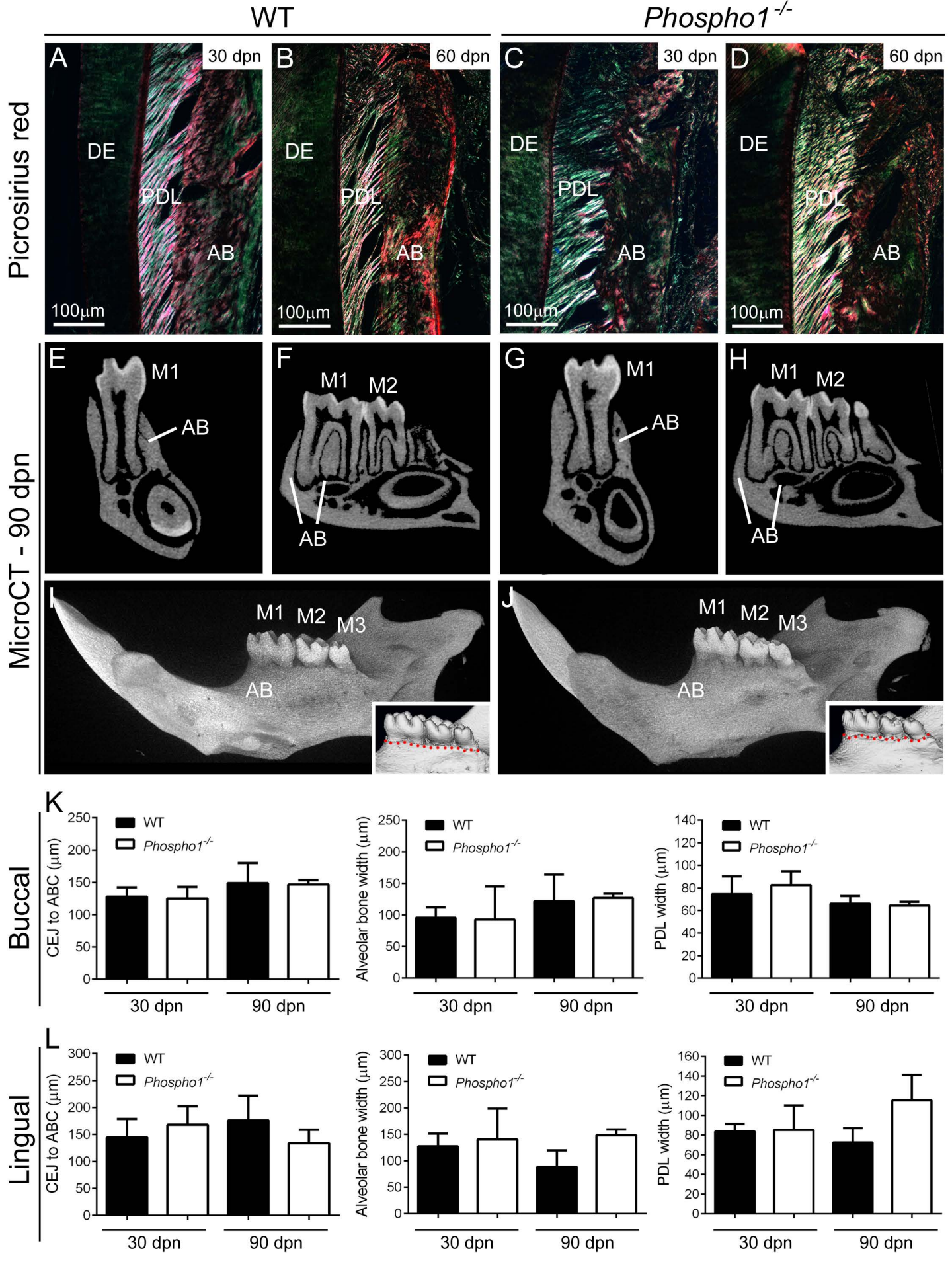
WT
Phospho1 -/-
Picrosirius red
A
30 dpn
B
60 dpn
C
30 dpn
D
60 dpn
DE
PDL
AB
100µm
MicroCT - 90 dpn
E
M1
AB
F
M1
M2
AB
G
M1
AB
H
M1
M2
AB
I
M1
M2
M3
AB
J
M1
M2
M3
AB
Buccal
K
WT
Phospho1 -/-
CEJ to ABC (µm)
Alveolar bone width (µm)
PDL width (µm)
30 dpn
90 dpn
Lingual
L
WT
Phospho1 -/-
CEJ to ABC (µm)
Alveolar bone width (µm)
PDL width (µm)
30 dpn
90 dpn

Supplemental Table 1. MicroCT analysis of dental tissues in *Phospho1*$^{-/-}$ vs. WT controls. Tissues were compared at 30 dpn. Values for WT, *Phospho1*$^{-/-}$, and *Phospho1*$^{-/-}$*; Spp1*$^{-/-}$ (n=5 each) samples are shown as mean ± standard deviation. No differences were found between WT and *Spp1*$^{-/-}$, therefore the latter sample values were not included with this data table.

Tissue	WT	*Phospho1*$^{-/-}$	*Phospho1*$^{-/-}$*; Spp1*$^{-/-}$
Alveolar bone			
TV (μm^3)	145.3 ± 19.8	138.8 ± 33.0	123.62 ± 16.6
BV (μm^3)	122.0 ± 19.9	104.9 ± 27.1	91.9 ± 14.0
BV/TV (%)	83.77 ± 0.04	75.23 ± 2.28 *	74.26 ± 2.69 *
TMD (mg HA/cm^3)	1025 ± 51	988 ± 9	977 ± 16
Dentin			
TV (μm^3)	405.3 ± 38.2	361.5 ± 14.2	367.6 ± 22.3
BV (μm^3)	353.3 ± 24.4	328.9 ± 14.6	326.1 ± 15.1
BV/TV (%)	87.37 ± 3.73	90.96 ± 0.90	88.78 ± 2.03
TMD (mg HA/cm^3)	1248 ± 55	1231 ± 27	1228 ± 7
Enamel			
TV (μm^3)	208.4 ± 8.2	194.2 ± 6.2	188.2 ± 11.2
BV (μm^3)	204.6 ± 8.8	191.0 ± 5.9	185.0 ± 11.0
BV/TV (%)	98.19 ± 0.54	98.34 ± 0.33	98.28 ± 0.26
TMD (mg HA/cm^3)	1909 ± 63	1860 ± 11	1886 ± 22
Thickness (μm)	63.4 ± 6.2	60.6 ± 1.8	60.0 ± 1.9

TV = Tissue volume
BV = Bone volume
TMD = Tissue mineral density
*$p < 0.05$ by independent samples t-test, compared to WT

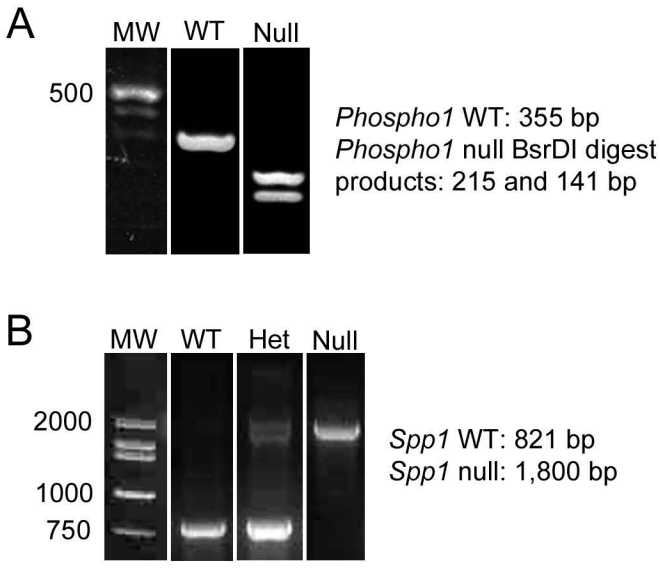
A
MW
WT
Null
500
Phospho1 WT: 355 bp
Phospho1 null BsrDI digest products: 215 and 141 bp
B
MW
WT
Het
Null
2000
1000
750
Spp1 WT: 821 bp
Spp1 null: 1,800 bp

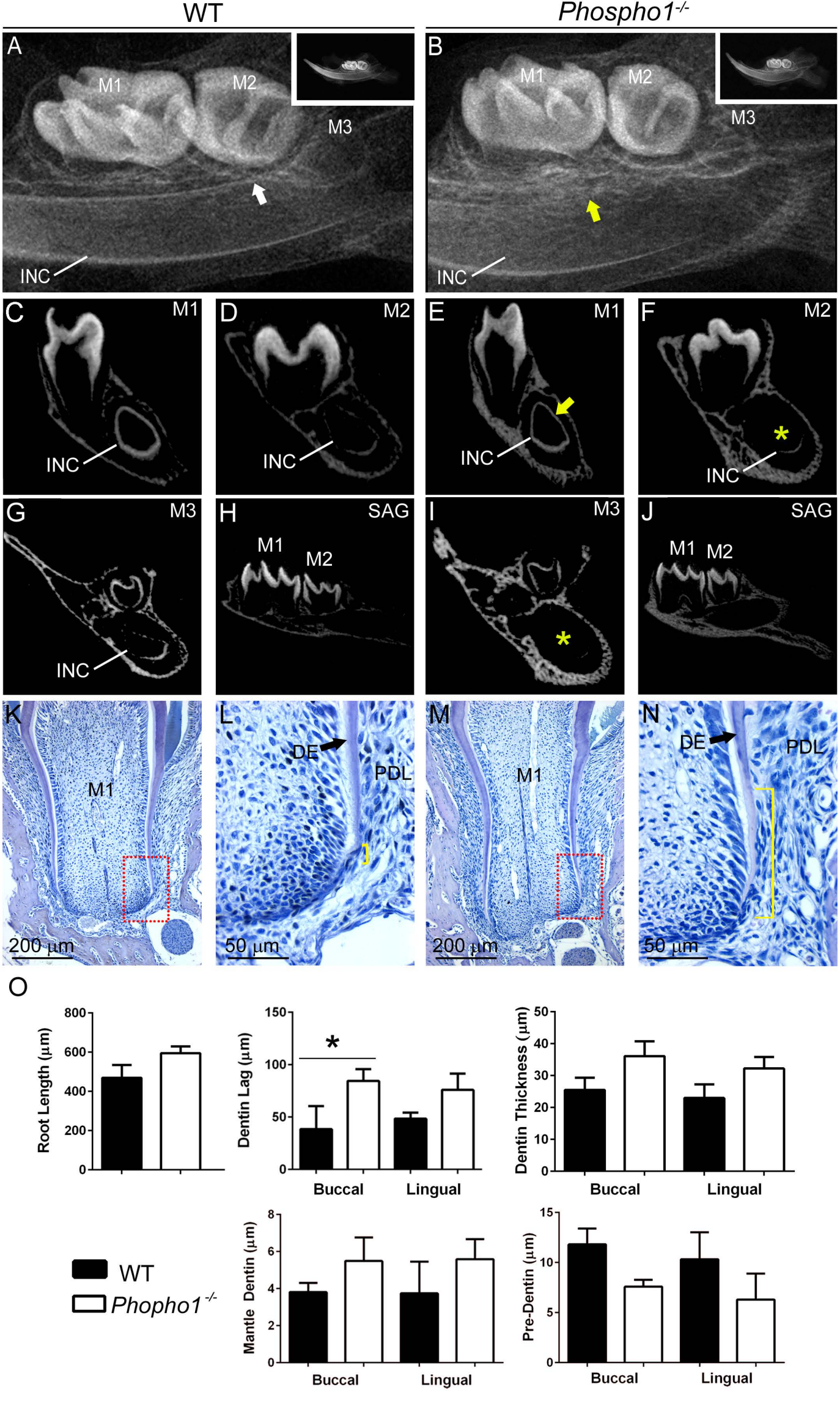
WT
Phospho1-/-
A
M1
M2
M3
INC
B
M1
M2
M3
INC
C
M1
INC
D
M2
INC
E
M1
INC
F
M2
*
INC
G
M3
INC
H
SAG
M1
M2
I
M3
*
J
SAG
M1
M2
K
M1
200 μm
L
DE
PDL
50 μm
M
M1
200 μm
N
DE
PDL
50 μm
O
Root Length (μm)
800
600
400
200
0
Dentin Lag (μm)
150
100
50
0
*
Buccal
Lingual
Dentin Thickness (μm)
50
40
30
20
10
0
Buccal
Lingual
WT
Phopho1-/-
Mantle Dentin (μm)
8
6
4
2
0
Buccal
Lingual
Pre-Dentin (μm)
15
10
5
0
Buccal
Lingual

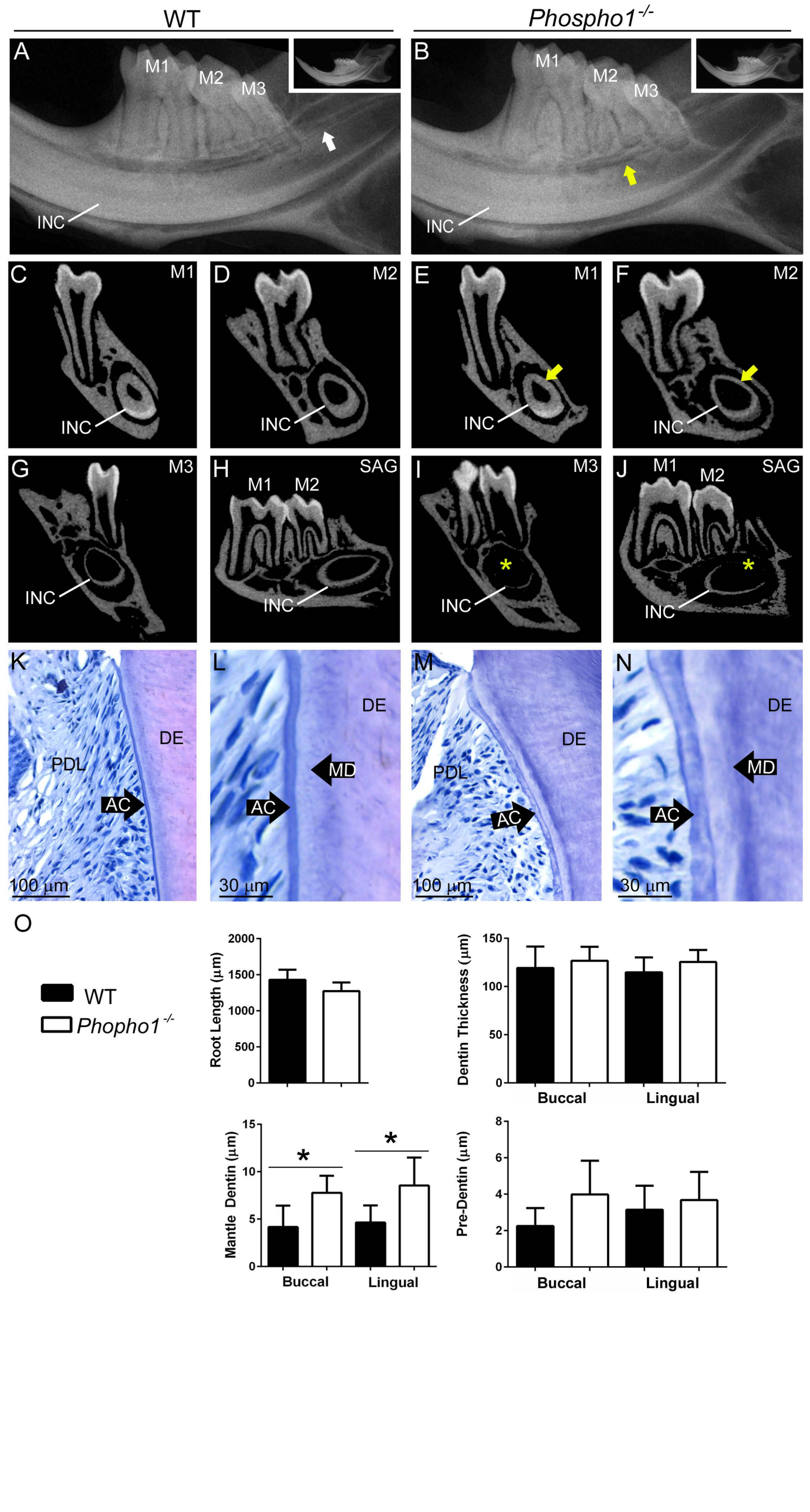
WT
Phospho1-/-
A
M1
M2
M3
INC
B
M1
M2
M3
INC
C
M1
INC
D
M2
INC
E
M1
INC
F
M2
INC
G
M3
INC
H
SAG
M1
M2
INC
I
M3
*
INC
J
M1
M2
SAG
*
INC
K
DE
PDL
AC
100 µm
L
DE
MD
AC
30 µm
M
DE
PDL
AC
100 µm
N
DE
MD
AC
30 µm
O
WT
Phospho1-/-
Root Length (µm)
2000
1500
1000
500
0
Dentin Thickness (µm)
150
100
50
0
Buccal
Lingual
Mantle Dentin (µm)
15
10
5
0
*
*
Buccal
Lingual
Pre-Dentin (µm)
8
6
4
2
0
Buccal
Lingual

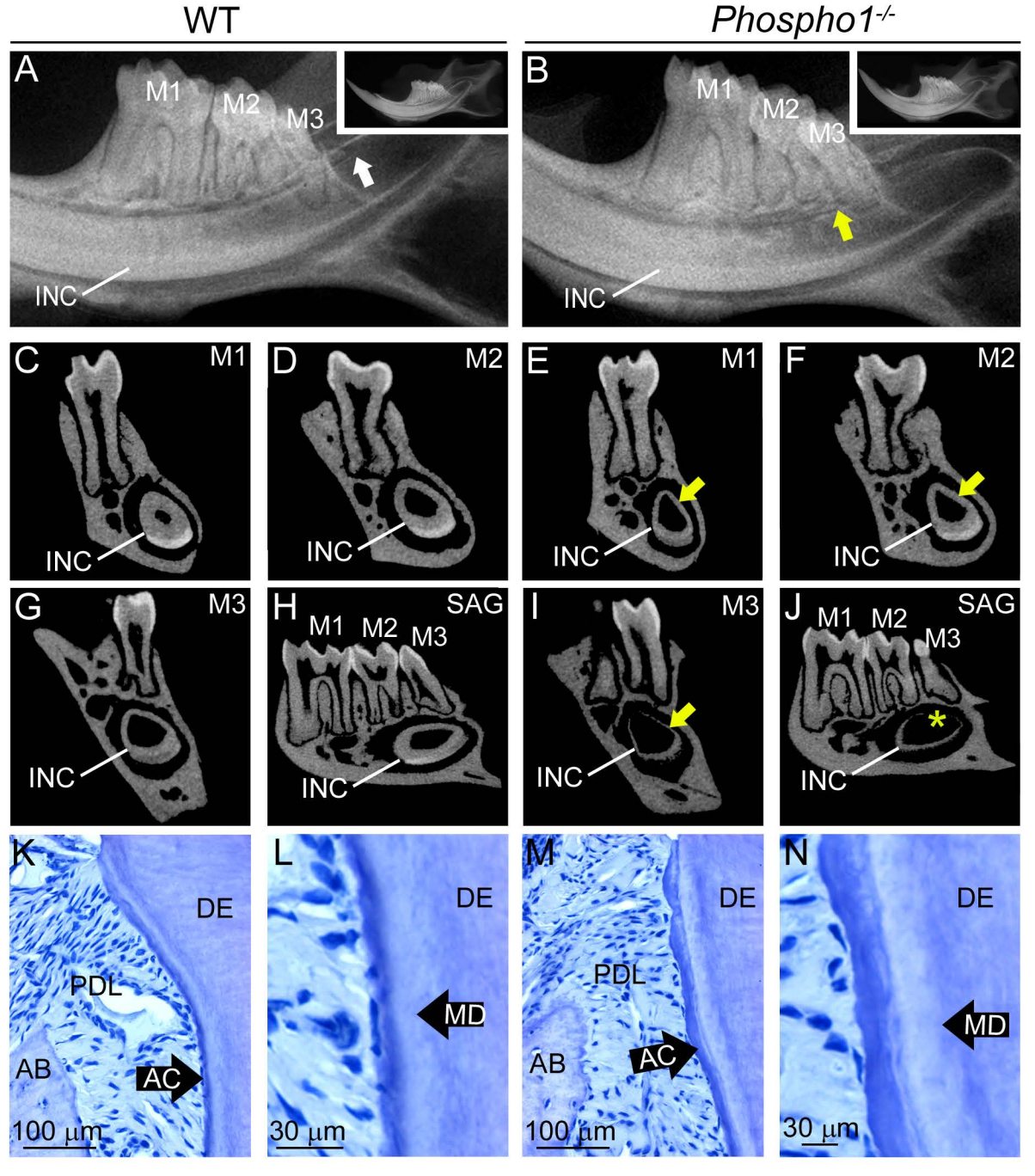
WT
Phospho1-/-
A
M1
M2
M3
INC
B
M1
M2
M3
INC
C
M1
INC
D
M2
INC
E
M1
INC
F
M2
INC
G
M3
INC
H
M1 M2 M3
SAG
INC
I
M3
INC
J
M1 M2
M3
SAG
*
INC
K
DE
PDL
AB
AC
100 µm
L
DE
MD
30 µm
M
DE
PDL
AB
AC
100 µm
N
DE
MD
30 µm

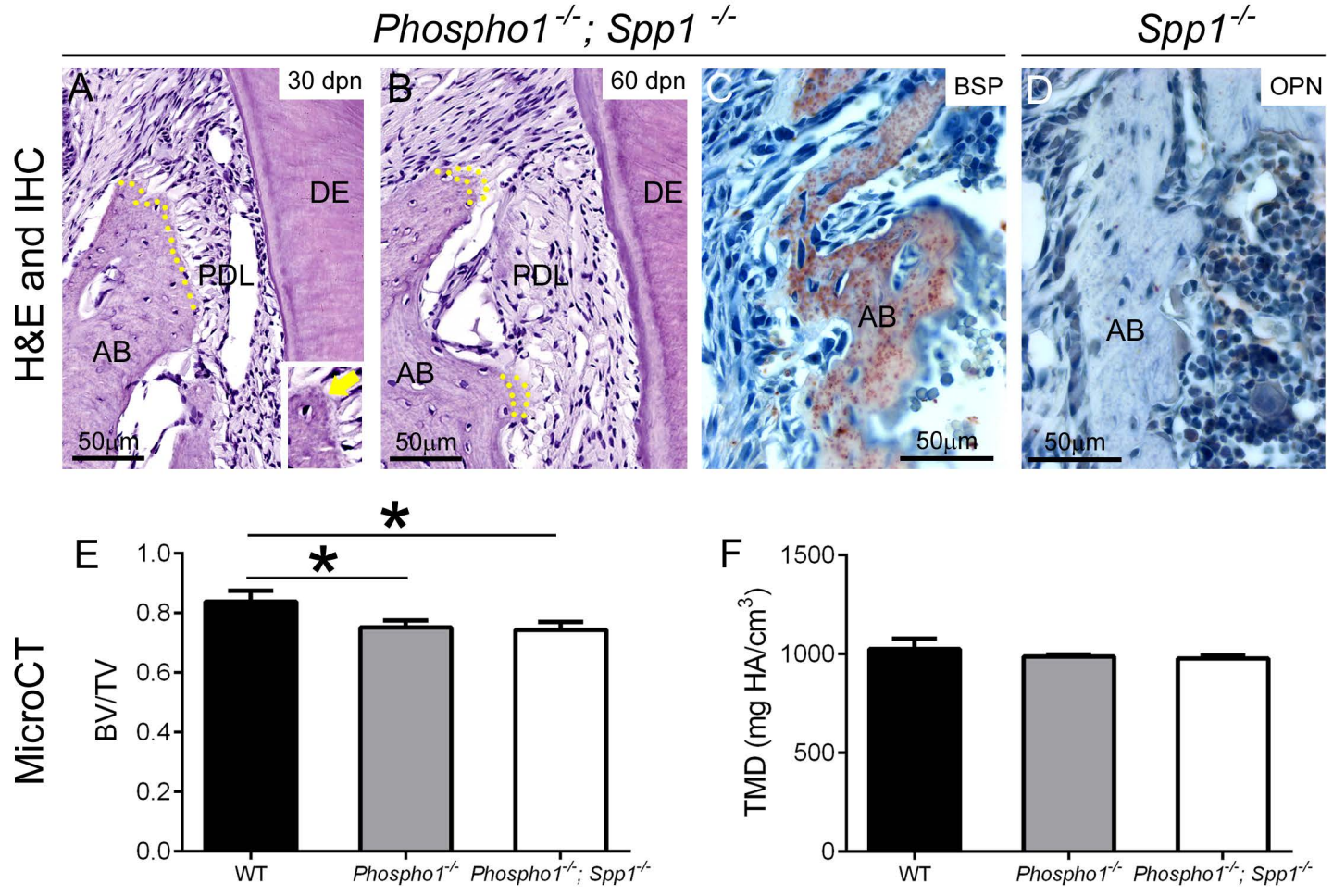
Phospho1-/-; Spp1 -/-
Spp1-/-
H&E and IHC
A
30 dpn
DE
PDL
AB
50µm
B
60 dpn
DE
PDL
AB
50µm
C
BSP
AB
50µm
D
OPN
AB
50µm

MicroCT
E
BV/TV
1.0
0.8
0.6
0.4
0.2
0.0
*
*
WT
Phospho1-/-
Phospho1-/-; Spp1-/-
F
TMD (mg HA/cm3)
1500
1000
500
0
WT
Phospho1-/-
Phospho1-/-; Spp1-/-

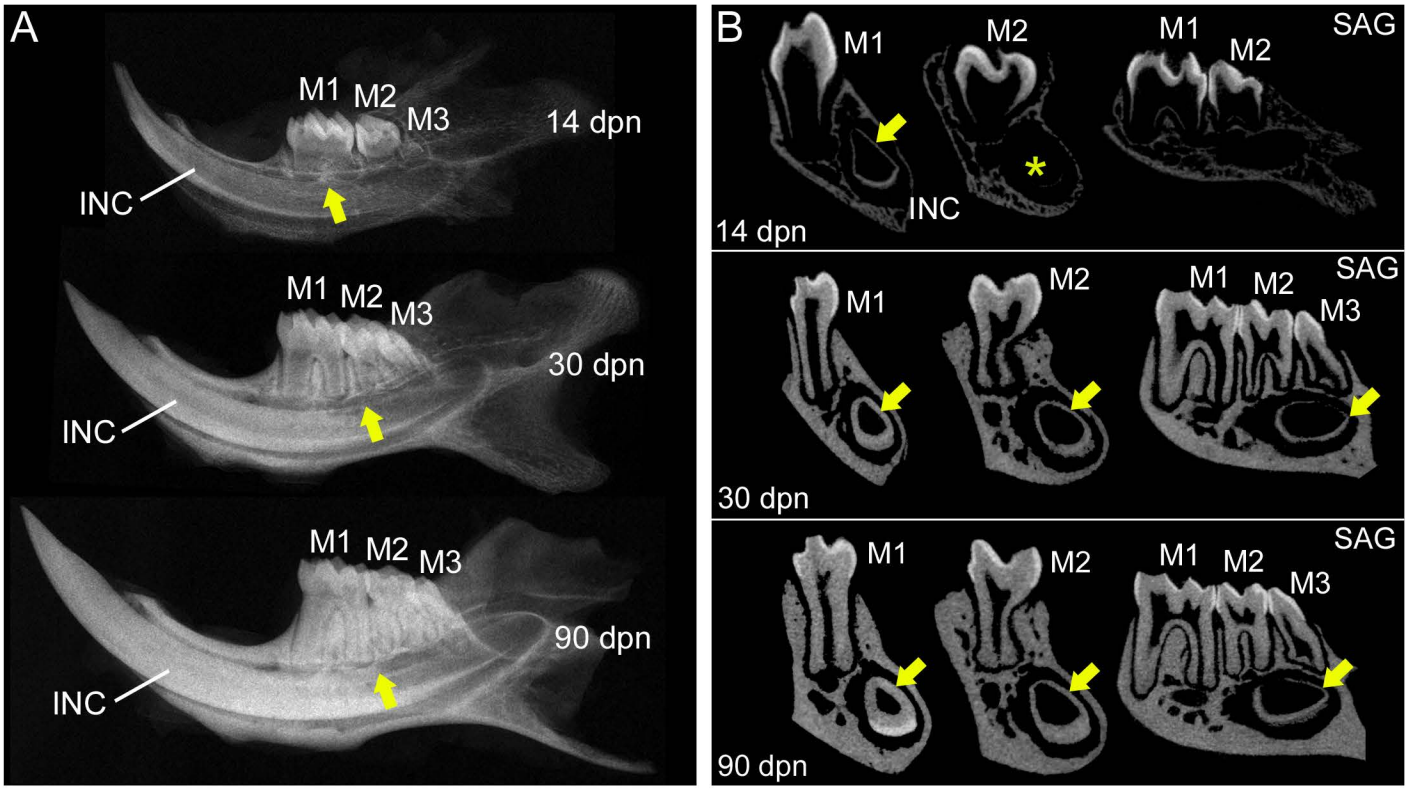
A
M1
M2
M3
14 dpn
INC
M1
M2
M3
30 dpn
INC
M1
M2
M3
90 dpn
INC
B
M1
M2
M1
M2
SAG
INC
14 dpn
M1
M2
M1
M2
M3
SAG
30 dpn
M1
M2
M1
M2
M3
SAG
90 dpn

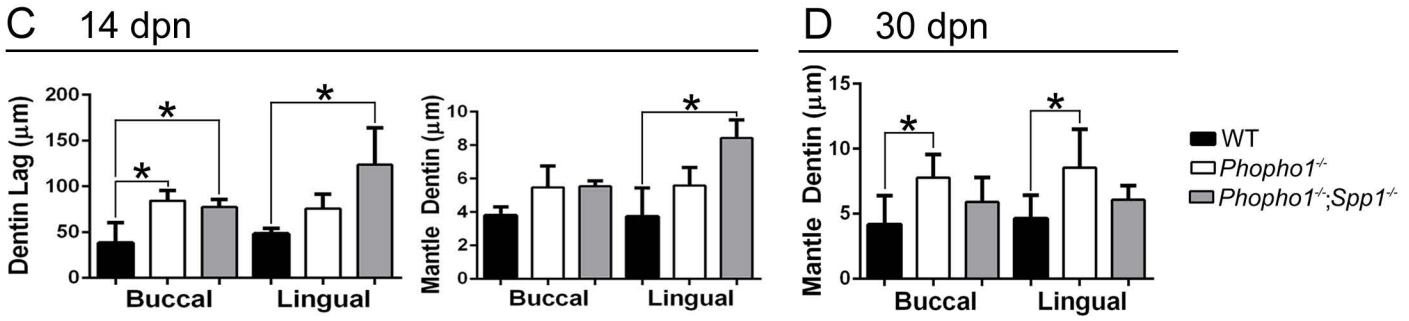
C 14 dpn
Dentin Lag (μm)
200
150
100
50
0
Buccal
Lingual
Mantle Dentin (μm)
10
8
6
4
2
0
Buccal
Lingual
D 30 dpn
Mantle Dentin (μm)
15
10
5
0
Buccal
Lingual
WT
Phopho1-/-
Phopho1-/-;Spp1-/-

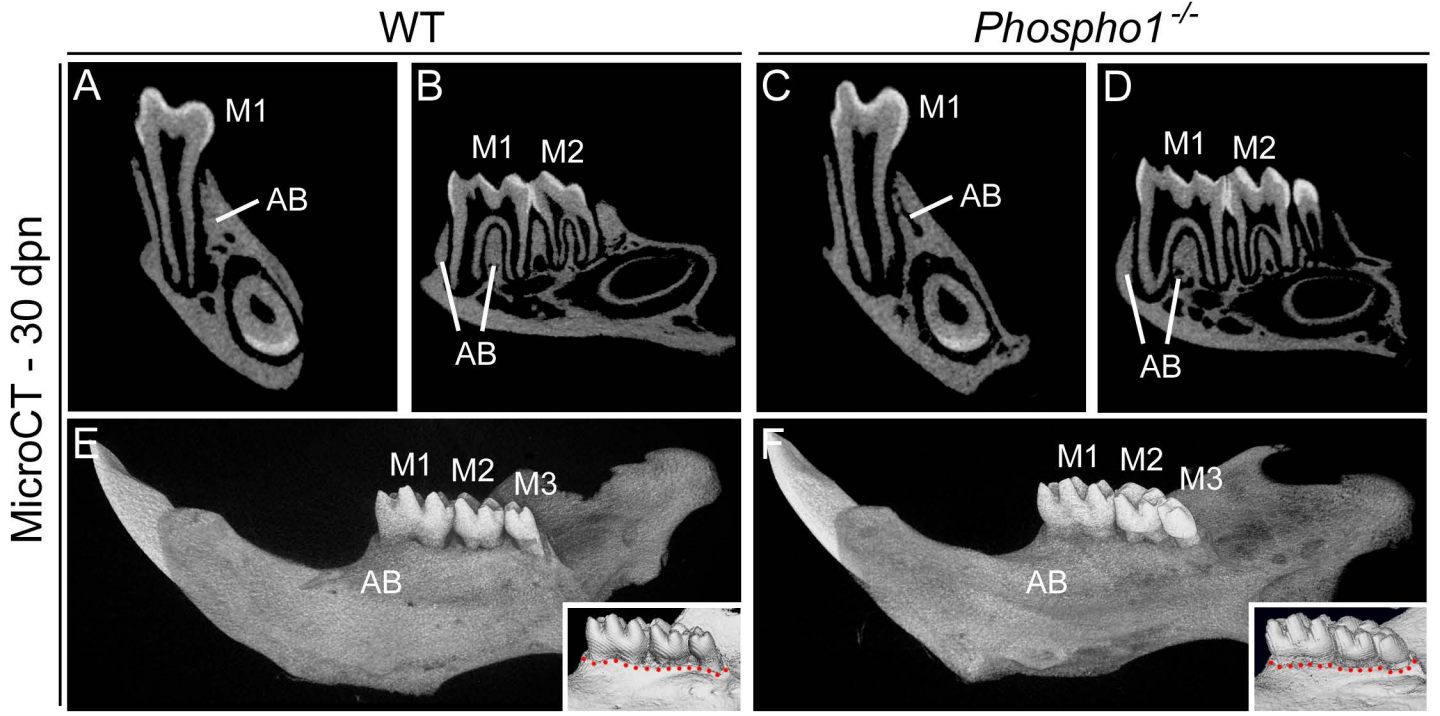
WT
Phospho1 -/-
MicroCT - 30 dpn
A
M1
AB
B
M1
M2
AB
C
M1
AB
D
M1
M2
AB
E
M1
M2
M3
AB
F
M1
M2
M3
AB